Neuro-Oncology Advances

4(1), 1–12, 2022 | https://doi.org/10.1093/noajnl/vdac135 | Advance Access date 23 August 2022

Low-level whole-brain radiation enhances theranostic potential of single-domain antibody fragments for human epidermal growth factor receptor type 2 (HER2)-positive brain metastases

Daniele Procissi[‡], Stephen A. Jannetti[†,‡], Markella Zannikou, Zhengyuan Zhou, Darryl McDougald, Deepak Kanojia, Hui Zhang, Kirsten Burdett, Ganesan Vaidyanathan, Michael R. Zalutsky, and Irina V. Balyasnikova

Department of Neurological Surgery, Northwestern University, Chicago, Illinois, USA (M.Z., D.K., I.V.B.); Department of Radiology, Northwestern University, Chicago, Illinois, USA (D.P.); Department of Preventive Medicine, Northwestern University, Chicago, Illinois, USA (H.Z., K.B.); Department of Radiology, Duke University Medical Center, Durham, North Carolina, USA (Z.Z., D.M., G.V., M.R.Z.)

[†]Present affiliation: Evergreen Theragnostics, Springfield, New Jersey 07081, USA

[‡]These authors contributed equally.

Corresponding Authors: Irina V. Balyasnikova, PhD, Department of Neurological Surgery, Northwestern University, Chicago, IL 60611, USA (irinabal@northwestern.edu); Michael R. Zalutsky, PhD, Department of Radiology, Duke University Medical Center, 311 Research Drive, Durham, NC 27710, USA (zalut001@mc.duke.edu).

Abstarct

Background. Single-domain antibody fragments (aka V_HH, ~ 13 kDa) are promising delivery systems for brain tumor theranostics; however, achieving efficient delivery of V_HH to intracranial lesions remains challenging due to the tumor–brain barrier. Here, we evaluate low-dose whole-brain irradiation as a strategy to increase the delivery of an anti- human epidermal growth factor receptor type 2 (HER2) V_HH to breast cancer-derived intracranial tumors in mice.

Methods. Mice with intracranial HER2-positive BT474BrM3 tumors received 10-Gy fractionated cranial irradiation and were evaluated by noninvasive imaging. Anti-HER2 V_HH 5F7 was labeled with ^{18}F, administered intravenously to irradiated mice and controls, and PET/CT imaging was conducted periodically after irradiation. Tumor uptake of ^{18}F-labeled 5F7 in irradiated and control mice was compared by PET/CT image analysis and correlated with tumor volumes. In addition, longitudinal dynamic contrast-enhanced MRI (DCE-MRI) was conducted to visualize and quantify the potential effects of radiation on tumor perfusion and permeability.

Results. Increased ^{18}F-labeled 5F7 intracranial tumor uptake was observed with PET in mice receiving cranial irradiation, with maximum tumor accumulation seen approximately 12 days post initial radiation treatment. No radiation-induced changes in HER2 expression were detected by Western blot, flow cytometry, or on tissue sections. DCE-MRI imaging demonstrated transiently increased tumor perfusion and permeability after irradiation, consistent with the higher tumor uptake of ^{18}F-labeled anti-HER2 5F7 in irradiated mice.

Conclusion. Low-level brain irradiation induces dynamic changes in tumor vasculature that increase the intracranial tumor delivery of an anti-HER2 V_HH, which could facilitate the use of radiolabeled V_HH to detect, monitor, and treat HER2-expressing brain metastases.

Key Points

- Low-level radiation enhances uptake of HER2-specific V_HH in intracranial tumors.
- XRT + radiolabeled V_HH shows promise as a treatment strategy for breast cancer brain metastases.

Importance of the Study

Improving the detection and treatment of brain metastases (BM) that over-express human epidermal growth factor receptor type 2 (HER2) is an urgent medical need. Drug delivery to BM is confounded by their tumor vasculature, which is more restrictive than in glioblastoma multiforme (GBM). Single-domain antibody fragments, about one-tenth the size of antibodies, could be promising theranostic vectors for BM provided sufficient BM uptake could be achieved. Here, we utilized longitudinal PET imaging to demonstrate that low-dose whole-brain irradiation (WBRT) significantly increased ^{18}F-labeled HER2-specific 5F7 V_HH uptake in intracranial HER2-positive tumors in mice. Our results suggest that combining low-dose WBRT with 5F7 V_HH labeled with therapeutic radionuclides could provide an effective strategy for treating patients with HER2-expressing BM.

Breast cancer affects approximately one in eight women and is the second leading cause of cancer death in women in the United States.[1] While systemic treatment has increased survival for metastatic breast cancer patients, the development of central nervous system (CNS) metastases in breast cancer patients is on the rise leading to a poor prognosis.[2–5] HER2 over-expression is found in approximately 30% of all breast cancer cases.[6,7] In HER2-positive patients, the rate of CNS metastases ranges from 30 to 50%,[8–10] making HER2 an attractive target for the detection and treatment of breast cancer brain metastases (BCBM).

In patients with BCBM, the blood–tumor barrier (BTB) hinders the delivery of clinically effective treatments. Despite being physically and heterogeneously impaired to a varying degree in almost all brain metastases, the BTB still effectively prevents significant tumor penetration of most chemotherapeutics and imaging agents in over 90% of cases.[11] The inability to reach the tumor tissue thus limits both the therapeutic and diagnostic efficacy of drug/agent-based approaches.

Whole-brain radiation therapy (WBRT) remains one of the most widely utilized treatment strategies for BCBM because it circumvents the BTB by providing a therapeutic effect without targeting tumor tissue via an exogenously administered agent.[12,13] WBRT, in conjunction with stereotactic radiosurgery, can provide a survival benefit, albeit only when treating single brain metastasis. The WBRT protocol consisted of 2.5–3 Gy daily doses over 10–15 days (30–37.5 Gy total dose), doses known to increase the permeability of the BBB in human patients diagnosed with brain metastases.[14,15]

The HER2-targeted monoclonal antibody (mAb) trastuzumab has permitted PET imaging of BCBM in patients,[16] however, generally only in those with significant BBB disruption resultant from a relatively high dose of WBRT or advanced tumors.

A promising strategy for circumventing this limitation is the development of smaller HER2-targeted scaffolds for PET imaging and radiopharmaceutical therapy, such as single-domain antibody fragments (aka V_HH or nanobodies). V_HH are derived from Camelids, have a molecular weight of 12–15 kDa, have low immunogenicity, and can have a sub-nanomolar affinity.[17,18] Importantly, studies in murine models with anti-HER2 V_HH have demonstrated considerably more rapid tumor penetration of V_HH compared with mAbs and the ability to localize in HER2-positive intracranial xenografts.[19] Moreover, the feasibility of imaging a patient with brain metastases using an anti-HER2 V_HH has been reported.[20]

The current study utilizes the anti-HER2 V_HH 5F7[21] to investigate the effects of low-level WBRT on its tumor uptake in an orthotopic BCBM mouse model using a noninvasive imaging approach. We hypothesize that by using WBRT fractions below 3 Gy, V_HH-based imaging agents and therapeutics could be made more effective without the quality of life impairments usually associated with higher radiation doses.[22] Importantly, the proposed strategy would enable clinicians to track transient changes in tumor physiology, including permeability, to identify optimal therapeutic and diagnostic windows.[14]

Methods

Cell Culture

HER2-overexpressing BT474BrM3 cells[23] (hereafter referred to as BT474Br) were originally obtained from Dr. D. Yu (MD Anderson Cancer Center) and modified via lentiviral transduction to express either firefly luciferase (fluc) or both fluc and mCherry fluorescent protein. Cells were maintained in DMEM media (Corning) supplemented with 10% FBS (HyClone, UT) and penicillin/streptomycin. BT474Br cells were tested for mouse pathogens and mycoplasma before using them in animal experiments.

Animal Studies

All animal studies were performed under protocols approved by the Institutional Animal Care and Use Committees at Northwestern University and Duke University. Six to eight-week-old female athymic nude mice were obtained from Jackson laboratories. Intracranial xenografts were established by injecting 4×10^5 BT474Brfluc cells in the right frontal lobe using a Hamilton syringe with a 26-gauge needle.[24] Following implantation, tumor growth was monitored by bioluminescent imaging.

Radiation Therapy

Mice with BT474Br intracranial xenografts were divided into control and irradiated groups. Mice in the irradiated group underwent WBRT for five consecutive daily 2-Gy doses using a GammaCell irradiator as previously described.[25]

Detailed procedures for radiolabeling 5F7, analysis of HER2 expression in tissue sections, and cells harvested from tumors by Western Blot and flow cytometry can be found in Supplementary Materials.

PET Imaging

PET/CT imaging was performed on a Siemens Inveon micro-PET/CT system (Malvern, PA). Mice were imaged 30 min post-i.v. injection of 1.5 ± 0.4 MBq (18.4 ± 10.9 μg) of ^{18}F-5F7. Mice were anesthetized using 2–3% isoflurane in oxygen and placed prone in the scanner gantry for a 5 min static PET acquisition followed by a 5 min CT scan. List mode PET data were histogram-processed, and images were reconstructed using a standard OSEM3D/MAP algorithm—2 OSEM3D iterations and 18 MAP iterations—with a cutoff (Nyquist) of 0.5. Images were corrected for attenuation (CT-based) and radioactive decay. Images were analyzed using Inveon Research Workplace software.

MRI and DCE-MRI Imaging

MRI was conducted on a 7T Bruker ClinScan. After placing a tail vein catheter for delivery of gadolinium (Gd^{3+}) contrast (average dose ~ 0.01 mmol/kg), each mouse was anesthetized using a mixture of O_2/100% and isoflurane and then placed in the scanner. Brain MR images were acquired using a dedicated brain 4-channel surface coil. Localization and anatomical reference were achieved using T2 weighted Turbo Spin Echo Sequences in all three geometrical orientations (axial, coronal, longitudinal). The same acquisition field-of-view (FOV) and geometric parameters, including the number of slices to cover the whole-brain (10–11), the slice thickness (0.5–1 mm), and the in-plane spatial resolution (~273 μm) were used for all 2D scans (including DCE-MRI) to facilitate postacquisition processing. The following sequences were used to obtain our MRI data: (1) gradient-echo sequences (GRE) with TR = 100 ms and TE = 2 ms and multiple flip-angles (FA = 5, 10, 15, 30, 45, 70, 80, 90) to acquire T1 maps of the brain before injection of contrast; (2) a GRE sequence with TR = ~50 ms and TE = ~2 ms repeated 100 times with a temporal resolution of ~3.6 s to obtain the DCE-MRI data. The injection of MR contrast was done as a bolus through a tail vein catheter around the 10th volume in order to follow the agent's vascular kinetics; (3) a 3D GRE sequence was then used to obtain images with 110 μm isotropic resolution. Following the transfer of DICOM images, postprocessing, extraction of T1 maps, and DCE-MRI processing were done using a built-in JIM 7.0 imaging software (Xinapse Systems). DCE-MRI processing involved using the T1 maps to obtain concentration from the MR image sequence and then using an automated arterial input function algorithm to calibrate the signal from different regions and tissues as described by Xinape Systems.[26] A model-independent voxel-by-voxel parametric map was then generated depicting the integrated area under the curve (IAUC) at different times after injection. The IAUC at 30 s and 120 s were selected to provide a semi-quantitative nonspecific measure of perfusion and permeability. Delineation of tumors in 2D and 3D MR images and parametric maps extracted from the DCE-MRI sequence was done using semi-automated threshold-based segmentation approaches included in ITK_SNAPsoftware. Tumor volumes were then obtained and expressed in mm^3.

Statistical Analysis

All statistical analyses were performed using Graphpad Prism 8 (GraphPad, San Diego, CA) or R statistical software version 4.0.2 along with extension package TOSTER (v 0.4.1). The sample size for each group was ≥3, and data were reported as mean ± SEM.[27] Multiple comparisons were done using one-way ANOVA, Tukey's multiple comparisons test. Comparisons between two groups were done using the two-sample *t*-test. *P* values were usually considered statistically significant if <.05 unless a Bonferroni Correction was applied to address multiple testing issues, and labeled as $*P < .05$, $**P < .01$, and $***P < .001$. The equivalence test[28] with 10% margin of means was performed for the HER2 expression data. Groups were considered to be equivalent when both *P*-value of two one-sided *t*-tests (TOST) were <.025, and not conclusive when either of these two *P*-values > .05. A Kaplan–Meier survival curve was generated to illustrate animal survival, and a log-rank test was applied to compare survival between control and irradiated mice.

Results

5F7 Binding to HER2 Expressing BT474Br Cells In Vitro and In Vivo

Staining of BT474Br cells in vitro with 5F7 and detection using anti-alpaca-biotinylated antibody and streptavidin-FITC revealed a positive signal compared to negative controls (Figure 1A). Flow cytometry analysis of 5F7 binding to live BT474Br cells incubated with and counter-stained with anti-alpaca-biotin, and streptavidin-FITC indicated that about 97% of cells were positive for HER2 expression (Figure 1B, C). The staining of BT474Br tumor tissue sections from mouse brain for HER2 with 5F7 further validated its binding to BT474Br cells ex vivo (Figure 1D, F, G). No binding of 5F7 was detected in normal brain tissue (Figure 1E, G), further validating the specificity of 5F7 binding to HER2-expressing BCBM.

^{18}F-5F7 Uptake In Intracranial BT474Br Xenografts

Radiochemical yields for the conjugation of [^{18}F]RL-III to 5F7 were 46.3 ± 7.7%; the molar activity of ^{18}F-5F7 was 6.9 ± 4.9 GBq/μmol. The effects of irradiation on the

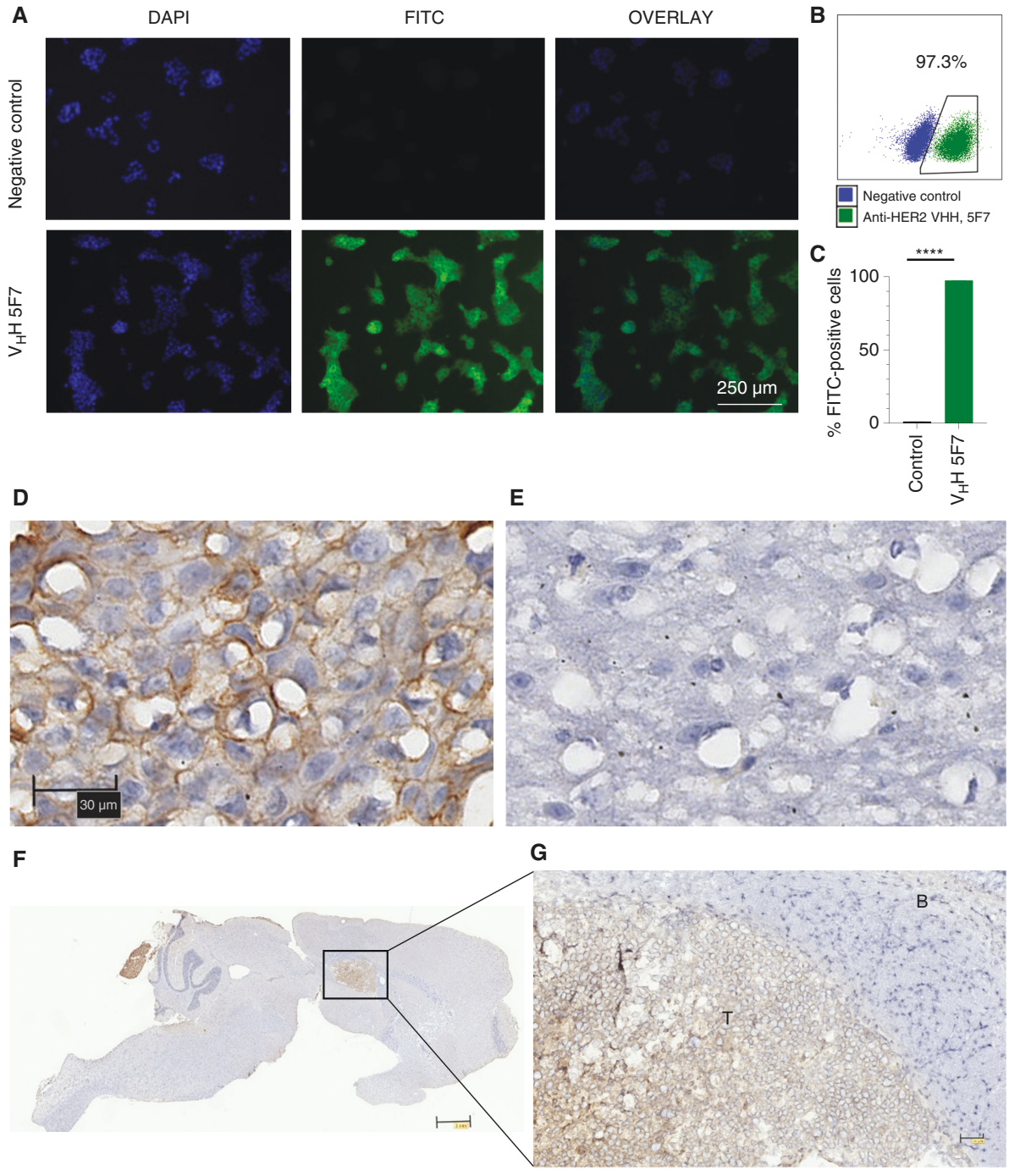

Figure 1. 5F7 binding to HER2-positive breast cancer brain metastasis cells. (A) Staining of BT474Br cells with 5F7 (4 µg/ml) and detection using anti-alpaca-biotinylated antibody and streptavidin-FITC. The scale bar is 250 µm. (B) Flow cytometry analysis of 5F7 binding at 1 µg/ml to live BT474BrM3 cells incubated with and counter-stained with anti-alpaca-biotin and streptavidin-FITC. (C) Quantitative analysis demonstrated that 94% of cells express HER2 ($n = 3$ per group). Staining with secondary antibody served as a negative control. Data presented as mean ± SEM, ****$P < .0001$. Unpaired *t*-test (D) H&E staining of BT474BrM3 tumor tissue section from mouse brain for HER2 with 5F7 (10 µg/ml) and biotinylated anti-alpaca antibody. Detection of secondary antibodies with streptavidin-peroxidase. The scale bar is 30 µm (E) negative staining of normal brain tissue from the frontal lobe. (F) 5F7 bound to tumor cells one hour after systemic delivery of 200 µg of 5F7 was detected using an anti-alpaca-biotinylated antibody and streptavidin-peroxidase on frozen, ice-cold acetone-fixed tissue sections. Specific stain seen in tumor but not in normal brain. Scale bar is 2 mm. (G) A higher power magnification of region from image F. T-tumor, B-normal brain. The scale bar is 100 µm.

uptake of ^{18}F-5F7 were evaluated by longitudinal PET imaging in two cohorts of mice—the first imaged on days 3 and 8 postirradiation and the second on days 12 and 18 postirradiation. No significant difference in tumor uptake between control and irradiated mice was observed until day 12 (irradiated, 2.18 ± 1.18 %ID/g; control. 0.00 ± 0.00 %ID/g, $^{**}P < .01$) (Figure 2A, B, D, E). On day 18, irradiated mice also displayed a greater tumor uptake (2.54 ± 1.53 %ID/g, $^{*}P < .05$) than controls (0.26 ± 0.58 %ID/g). Plotting ^{18}F-5F7 uptake versus tumor volume revealed a similar deviation from zero in slopes between control ($P = .013$) and irradiated groups on day 8 ($P = .051$), with a significant slope difference being observed in the irradiated group (deviation from zero, $P = .012$) on day 18 (Figure 2C, F).

HER2 Expression in BT474Br Xenografts: Control vs. Irradiated Mice

We next investigated whether differences in ^{18}F-5F7 tumor uptake between control and irradiated mice were associated with altered HER2 expression. After the last PET

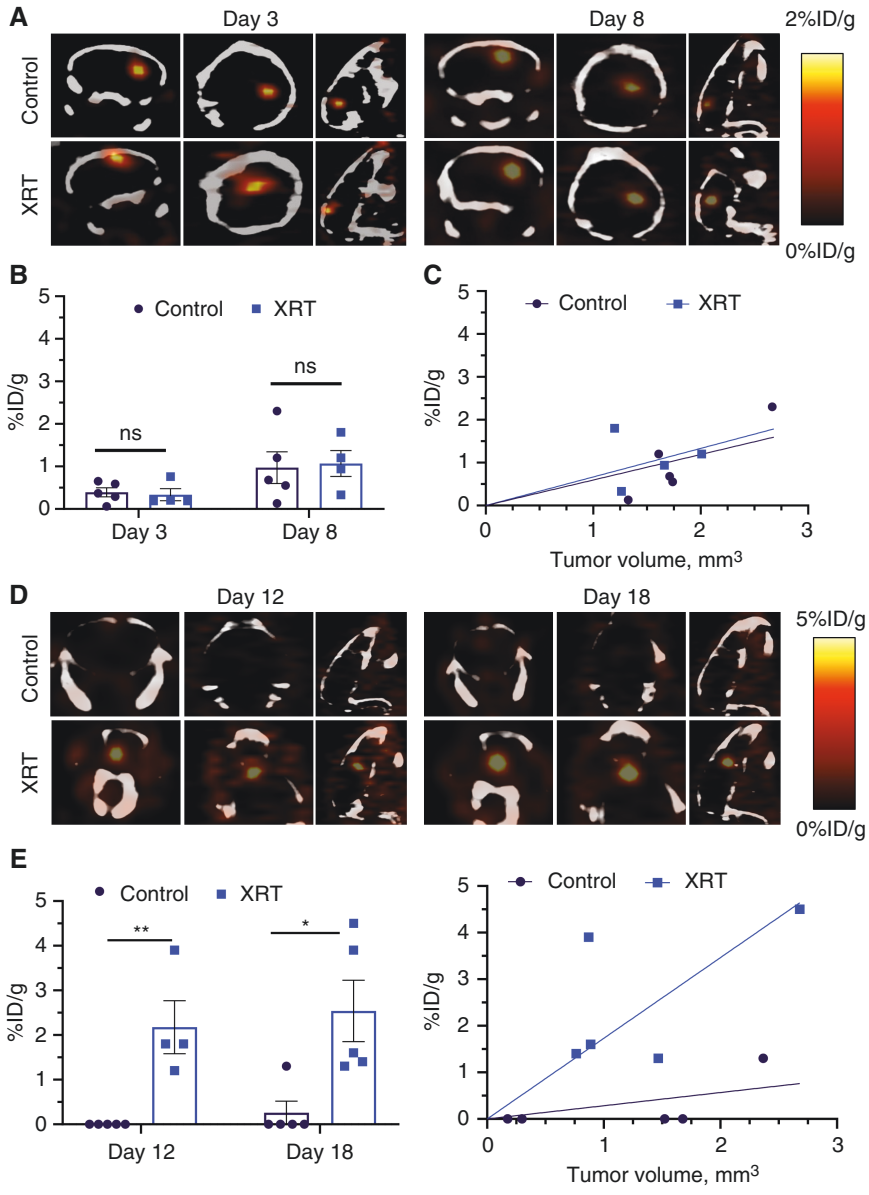

Figure 2. MicroPET/CT imaging of ^{18}F-5F7 distribution in mice with intracranial BT474Br xenografts. Cohort 1: days 3 and 8 postirradiation. (A) MicroPET/CT scans of representative control ($n = 5$) and irradiated mice ($n = 4$). (B) ^{18}F-5F7 uptake (% ID/g). (C) ^{18}F-5F7 uptake vs. tumor size (determined by morphometry on tissue sections). Cohort 2: days 12 and 18 postirradiation. (D) MicroPET/CT scans of representative control ($n = 5$) and irradiated mice ($n = 4$). (E) ^{18}F-5F7 uptake (% ID/g). (F) [^{18}F]5F7 uptake vs. tumor volume. Data presented as mean ± SEM, $^{*}P < .05$; $^{**}P < .01$. Two-sample *t*-test.

imaging session on day 18, tissue sections from paraffin-embedded brains (n = 3 from both the irradiated and control groups) were obtained and evaluated for HER2 expression. No qualitative or quantitative differences in HER2 expression were observed between control and irradiated BT474Br xenografts (Figure 3A). Western blot analysis of cells from the brain tumors obtained 2 days after irradiation (n = 4) and corresponding controls was performed to confirm these results; no significant difference was detected in total HER2 expression in BT474Br tissue between control and irradiated groups (P = .74, two-sample t-test, whereas TOST upper P-value = .036 and TOST lower P-value = .086 with 10% margin of mean) (Figure 3B). Similarly, flow cytometry showed no conclusion in difference in HER2 expression on BT474Br cells harvested from the brains of control and irradiated mice per both two-sample t-test and equivalance test (Figure 3C(a)). There was an estimated small 7.4% difference in the mean fluorescence intensity of bound antibodies (Figure 3C(b)) between BT474Br cells harvested from control and irradiated animals (*P < .05, two-sample t-test). Taken together, the data collected from tissue sections on day 18 suggest that WBRT does not change HER2 expression in intracranial BT474Br xenografts, whereas data collected from the HER2 analysis by western blot and flow cytometry at an earlier time point after WBRT were not conclusive.

MRI Evaluation of BT474Br Tumor Volume and Vascular Status

MRI-based BT474Br tumor volumetric analysis was performed to evaluate temporal changes in tumor volume in response to WBRT. Figure 4A (a) shows a representative slice of a mouse brain from the 3D MRI data set with the tumor region depicted in red color. The corresponding rendered 3D images (b, c) depict two views of the head/brain outline and 3D tumor morphology, illustrating the ability to visualize the location, size, and morphology of the tumor lesion. The average tumor volume at 3, 7, and 17 days after irradiation did not change significantly in the treated group; however, there was a significant increase in size in the control group on day 17 (Figure 4B). Although MRI indicated a difference in tumor volume between control and irradiated mice on day 17, there was no difference in median survival between these two groups (Figure 4C). Representative control and irradiated mouse MR images with superimposed parametric IAUC maps extracted from the DCE-MRI data are shown in Figure 5A. The longitudinal parametric changes in tumor perfusion/permeability compared to normal brain consistently exhibited a markedly more heterogeneous and often larger increase in both IAUC30 (integrated area under the curve at 30 s) and IAUC120 (IACUC at 120 s) in the irradiated group compared to the controls, especially at 7 days postirradiation (Figure 5B, C). Tumor IAUC values were consistently higher than for normal brains in both treated and control animals. The longitudinal changes observed in the irradiated mice suggest more heterogeneous intra-tumoral micro-environment alterations than in the control mice. The longitudinal changes observed in tumor IAUC30 were statistically different between the two cohorts (compared to the preradiation baseline value), but the IAUC120 were not, although an increasing trend was seen. Although the effect of radiation on tumor vasculature parameters was consistently observed, a comparison of average whole-tumor values fails to capture the complex changes induced. This is illustrated in the 2D, and the corresponding 3D Intra-tumor vascular variability maps (Figure 6), demonstrating more heterogeneous behavior in irradiated mice, particularly in the 3D rendered images.

Discussion

Treatment of BM is challenging due to the need to spare healthy normal brain tissue while achieving adequate drug transport across the BTB to have sufficient therapeutic effect. HER2 targeting via V_HH molecules offers a promising approach for targeting radiation to HER2-positive cancers, as demonstrated by studies with 5F7 labeled with both the therapeutic radionuclides ^{131}I[21] and ^{211}At[29] and ^{18}F for PET imaging.[19] Likewise, radiolabeled V_HH tumor targeting of therapeutic and PET radionuclides also has been demonstrated with 2Rs15d, an anti-HER2 V_HH, which binds to a different epitope on the HER2 extracellular domain than 5F7[19,30] and has recently entered clinical investigation.[31] Studies with radiolabeled 2Rs15d confirmed the ability to target intracranial tumors in mice[32]; however, the therapeutic effect was modest even with 3 doses of ^{225}Ac-2Rs15d, which emits 4 α-particles per decay.

In order to evaluate whether low-dose WBRT could augment V_HH uptake in intracranial xenografts, we utilized the HER2-positive brain metastatic breast cancer line, BT474Br.[33,34] We first validated that 5F7 efficiently binds to HER2 on BT474Br cells in vitro by immunocytochemistry and flow cytometry. Positive and specific detection of HER2-expressing BT474Br cells in xenografts but not normal brain also was evident on tissue sections. Furthermore, 5F7 accumulated in tumor tissue but not in the normal brain after i.v. delivery, confirming that this V_HH is suitable for imaging HER2-positive BCBM.

We selected WBRT as a strategy for enhancing the potential utility of radiolabeled V_HH for the detection and treatment of BCBM. Patients undergoing WBRT for treatment of brain metastases typically receive 2.5–3 Gy daily dose fractions for a total of 30–37.5 Gy.[35] In our experiments, mice were subjected to a fractionated WBRT of 10 Gy (5 × 2 Gy daily) regimen in order to evaluate a dose likely to avoid neurotoxicity in patients, which occurs at higher doses of WBRT in patients with BCBM.[36,37] In addition, we employed longitudinal PET imaging with ^{18}F-5F7 to quantify tumor delivery noninvasively in the same animals at multiple time points after irradiation. As expected, at this radiation dose, WBRT did not improve the survival of the mice. However, we observed a significant increase in ^{18}F-5F7 V_HH uptake beginning 12 days after WBRT completion compared to nonirradiated mice. Furthermore, the enhanced uptake of the 5F7 V_HH was more pronounced on day 18 after WBRT motivating future studies to define the post-WBRT time when uptake enhancement would occur.

Radiotherapy can change gene expression in several cell types within a tumor and a normal brain.[38,39] To ensure that the increase in ^{18}F-5F7 uptake was not due to WBRT-induced

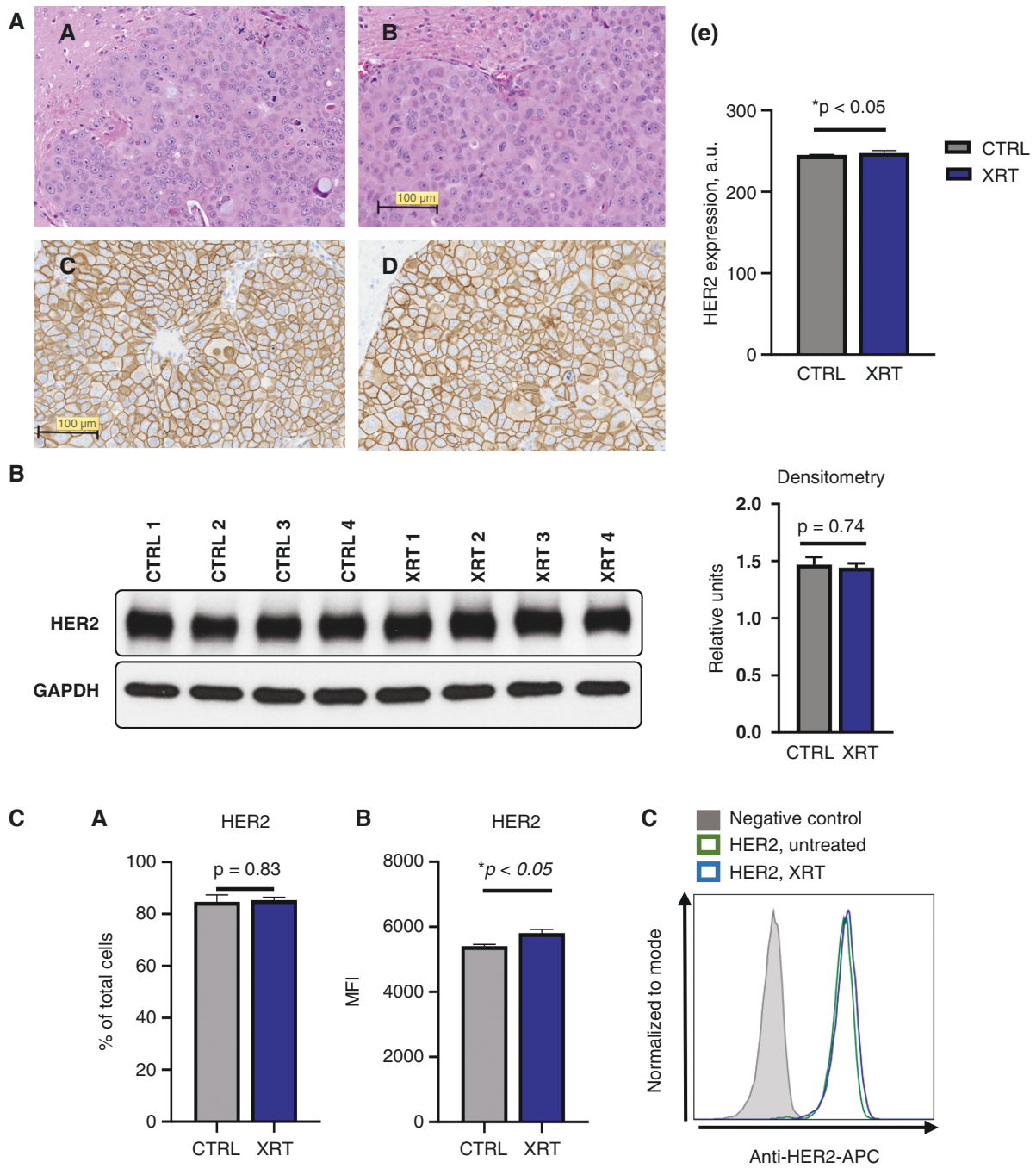

Figure 3. Analysis of HER2 expression in BCBM BT474Br model after WBRT by three complementary approaches—western blot, flow cytometry, and immunohistochemistry. (A) H&E stain of a representative brain section from control (a) and irradiated mice (b) and corresponding immunostaining for HER2 expression from control (c) and irradiated (d) mice. The scale bar is 100 µm. (e) quantitative analysis of HER2 expression in stained tissue sections (3 animals per group). Data presented as mean ± SEM. Significance level .05, equivalence test with 10% margin of the mean. (B) HER2 expression in cells harvested from BT474Br tumors after 5 × 2 Gy daily WBRT and controls by western blot analysis. Densitometry of HER2 and GAPDH performed and calculated as a ratio show no significant difference between HER2 expression in control and irradiated animals. (n = 4 per group; mean ± SD, P = .74, Student's t-test). (C) HER2-expression analysis on BT474Br cells harvested from control and irradiated tumors by flow cytometry. Results expressed as (a) % positive cells (n = 4 per group; mean ± SEM, P = .83, two-sample t-test) and (b) median fluorescent intensity (MFI) (n = 4 per group; mean ± SEM, P < .05, two-sample t-test). A representative flow histogram (c) is shown on the right.

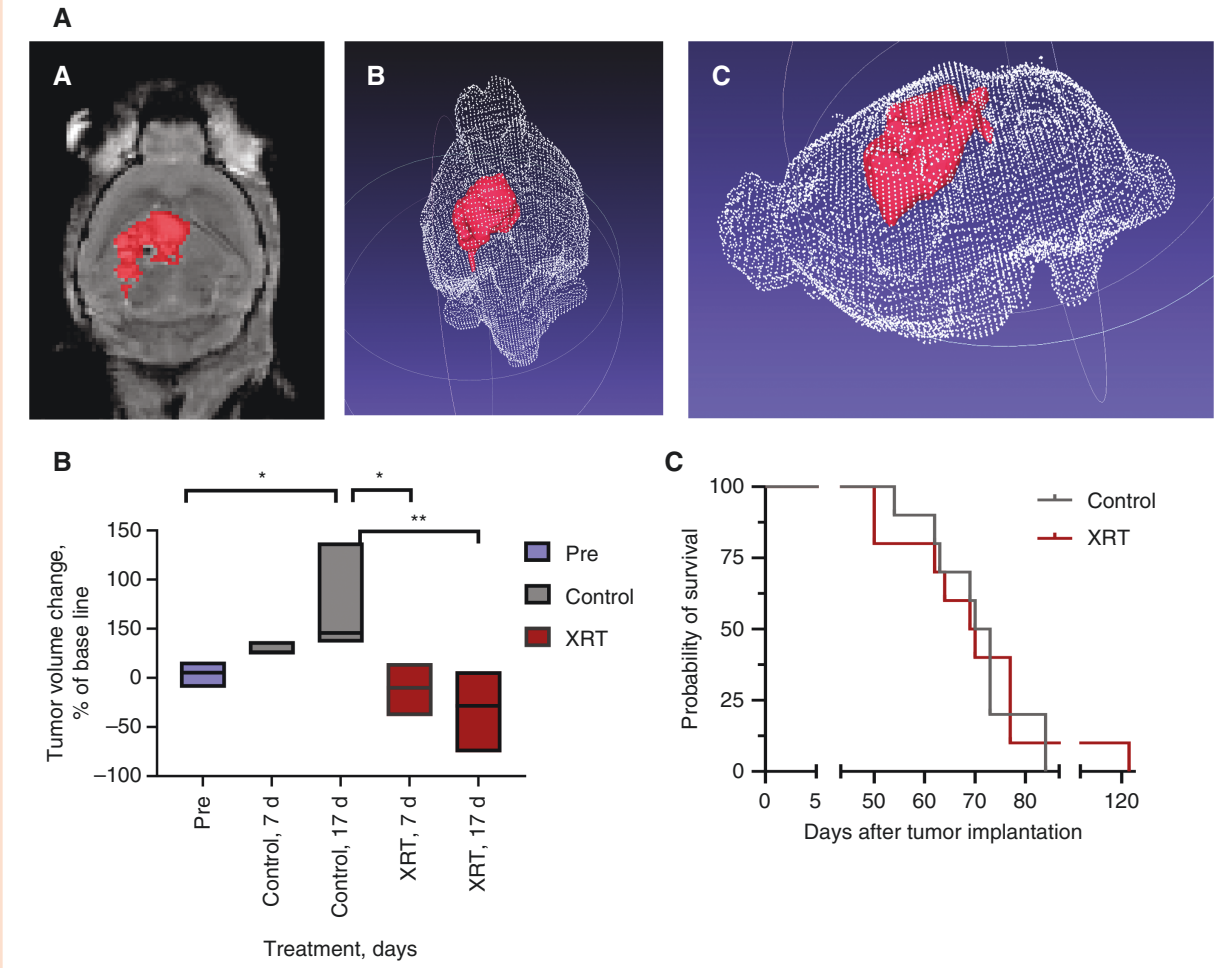

Figure 4. Effect of WBRT on tumor volume and survival. (A) (a) T2 MRI visualizes BT474Br intracranial tumor in 2D (a) and two 3D (b, c) views. (B) Tumor volume changes post-WBRT compared to untreated controls. (C). Survival analysis shows no significant difference between irradiated and control groups. Data presented as data range with line showing median. *$P < .05$; **$P < .01$. One-way ANOVA, Tukey's multiple comparisons test.

alterations in HER2 expression, we analyzed the HER2 levels in tumor tissue obtained immediately after completion of the PET experiment. H&E staining of tissue sections confirmed tumor presence in both irradiated and control mice. The measurement of HER2 expression levels in tissue sections revealed no difference between the groups, confirming that the higher uptake of ^{18}F-5F7 in the tumors of irradiated mice is probably not due to changes in HER2 expression. Consistent with the well-known effects of radiation on tumor vasculature,[40–42] it is likely that the higher uptake of ^{18}F-5F7 in irradiated tumors reflects their higher permeability.

To gain further insights into the effects of WBRT on ^{18}F-5F7 uptake in intracranial BT474Br xenograft, we utilized DCE-MRI with Gd^{3+} contrast to assess BTB permeability in irradiated and control mice. MRI provided a volumetric comparison of tumors, which demonstrated a significant increase in tumors' growth in control but not WBRT groups at day 17 but not at earlier time points. In contrast, we observed greater tumor perfusion and permeability of contrast agent in irradiated tumors with DCE-MRI than in nonirradiated controls. The difference in permeability between control and irradiated animals was apparent about a week after treatment, with more distinction on day 17 after WBRT. The changes in the permeability of BT474Br BCBM after irradiation correlated with a greater uptake of ^{18}F-5F7, particularly at the latest time points analyzed in our study. Our data are consistent with a previous report where patients with brain metastases had an increase in gefitinib uptake with increasing doses of WBRT up to 30 Gy.[43] In addition, several studies in preclinical mouse models have found that BCBM lesion volume does not correlate with passive permeability.[11,44,45]

The number of lesions in BCBM patients can vary significantly from a single lesion to greater than 10, which is a factor in determining a treatment regimen. WBRT, the most prevalent treatment, is performed at different intervals to mitigate the associated neurocognitive decline.[46] In a 30-patient study, the permeability of metastatic brain lesions was found to be variable and could be increased to varying degrees about 2–4 weeks after WBRT or stereotactic radiosurgery.[15] Although not investigated in depth in this study, our DCE-MRI imaging revealed heterogeneity in the

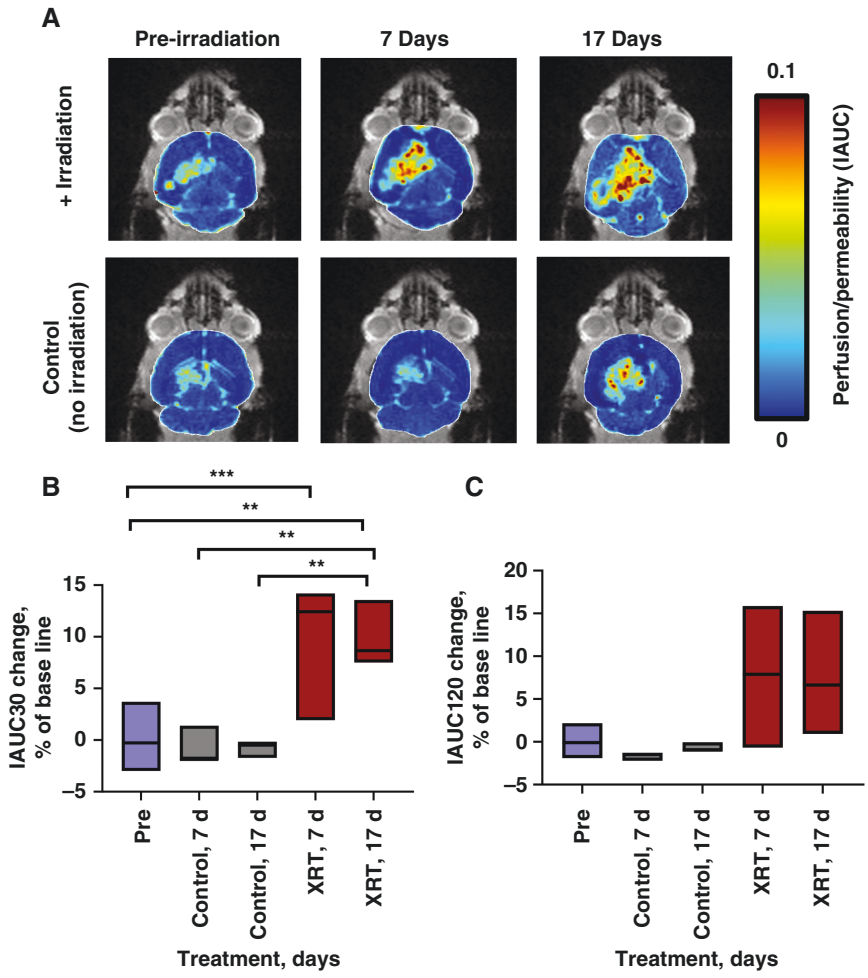

Figure 5. Tumor perfusion and permeability visualization, and IAUC30 and IAUC120 parameters from DCE-MRI data. (A) IAUC parametric color maps of the brain and tumor of representative mice from irradiated and control groups superimposed on anatomical MRI for reference. Vascular changes in tumors and normal brain due to WBRT are readily visualized. The average percent short (B; IAUC30) and long (C; IAUC120)-time uptake and washout kinetics of contrast were determined in mice before (baseline) and at 7 and 17 days postirradiation. Data presented as data range with a line showing the median. $^*P < .05$; $^{**}P < .01$; $^{***}P < .001$. One-way ANOVA, Tukey's multiple comparisons test.

perfusion/vascular permeability alterations induced by the irradiation of BT474Br tumors.

Nevertheless, by increasing the permeability of BCBM and addressing the heterogeneous response of tumor vasculature to irradiation, we may unlock the potential for administering more targeted therapies to these patients. This could avoid the need for WBRT at doses causing unwanted side effects that compromise the quality of life. Considering the type of vehicle for tumor targeting, the permeability requirements for V_HH should be favorable due to their considerably smaller size compared to intact antibodies. Although WBRT is known to enhance the permeability of the brain-tumor-barrier in both animal models and patients, its effects have not yet been validated for use with small protein molecules like V_HH. Studies in animal models have demonstrated that the BTB in brain metastases is more restrictive than in glioblastoma,[47] making V_HH a relevant carrier system for theranostic approaches for brain metastases. Future work will explore these requirements as we look to define the optimal XRT regimen for increasing permeability without inflicting irreversible damage to the normal brain.

Overcoming the BTB would allow new diagnostic tools to detect metastases that would otherwise remain undiscovered with existing strategies. In addition, a greater diagnostic toolbox would better inform the selection of treatment regimens. In conclusion, ^{18}F-5F7 V_HH exhibited enhanced tumor accumulation in a HER2-expressing BCBM model when preceded by low-dose WBRT, which correlated with increased perfusion and permeability and was not linked to changes in HER2 expression. These studies suggest the potential utility of the V_HH PET tracer, ^{18}F-5F7, as an imaging tool for HER2-positive BCBM. The novelty lies in the ability of 5F7 V_HH to target brain lesions and not normal brain after WBRT and the added opportunity to use DCE-MRI to visualize and quantify changes in vascular parameters in this context. The knowledge we gained in this study could be optimized for therapeutic intervention to increase the uptake of

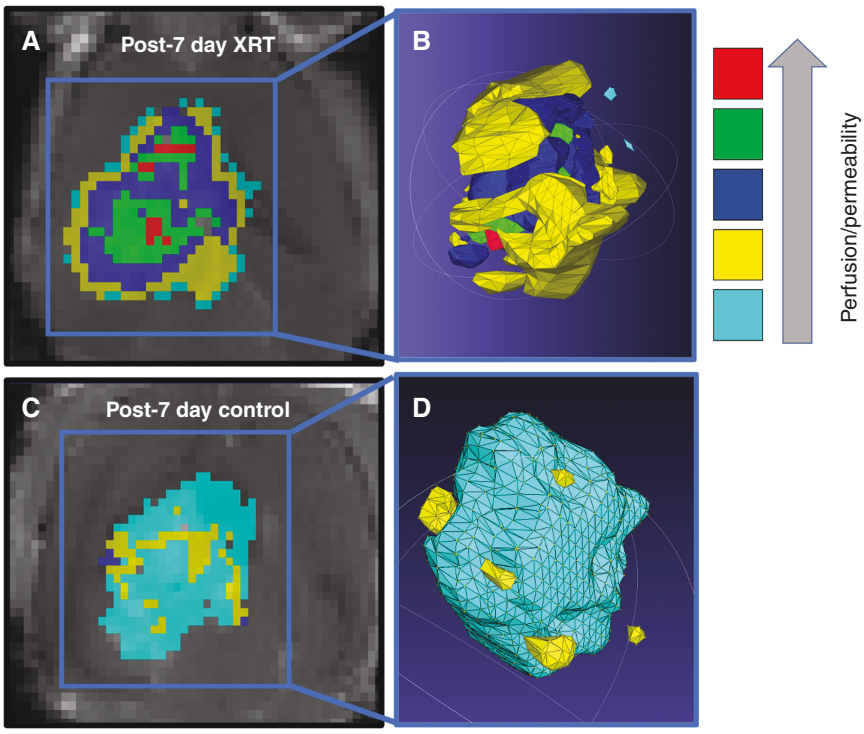

Figure 6. Visualization of intra-tumor perfusion and permeability heterogeneity on day 7. IAUC120 derived color maps quantitatively segmented and superimposed on the corresponding MRI anatomical images for representative irradiated (a) and control (c) mouse illustrating intra-tumoral patterns of perfusion/permeability. The corresponding 3D renderings (b, irradiated; d, control) enable 3D visualization of radiation-induced heterogeneities in the tumor microenvironment.

V_HH carrier molecules labeled for imaging and potentially therapeutic radionuclides.[48] These results bring us closer to understanding how BTB permeability can be increased to deliver small proteins like V_HH to BCBM and warrant further investigation.

Supplementary Material

Supplementary material is available at *Neuro-Oncology Advances* online.

Keywords

breast cancer brain metastases | HER2 | PET | single-domain antibody fragment | V_HH.

Funding

This work was supported by a Lynn Sage Cancer Research Foundation grant (I.V.B.), National Institute of Health/National Cancer Institute grants CA42324 (M.R.Z.) and CA188177 (G.V.).

Acknowledgments

The authors are grateful to the Mouse Histology and Phenotyping Core Facility, Northwestern University, for assistance with processing and staining mouse tissues.

Conflict of interest statement. G.V., M.R.Z., and Z.Z. are inventors on a patent application describing the RL-III ^{18}F labeling technology licensed by Zentera Alpha from Duke University. The other authors disclosed no potential conflict of interest.

Authorship statement. Study design: M.R.Z. and I.V.B. MRI data collection and analysis: D.P. Radiochemistry: Z.Z., D.M., and G.V. PET imaging data collection and analysis: Z.Z and S.A.J. Histology, Flow Cytometry and Western Blot: I.V.B., M.Z, D.K. Statistical analysis: H.Z., K.B. Final manuscript review: I.V.B. and M.R.Z.

References

1. Howlader N, Noone AM, Krapcho M, et al., eds. *SEER Cancer Statistics Review, 1975–2018*. Bethesda, MD: National Cancer Institute; 2013. https://seer.cancer.gov/csr/1975_2018/, based on November 2020 SEER data submission, posted to the SEER web site, April 2021. Accessed April 2022.
2. Giordano SH, Buzdar AU, Smith TL, et al. Is breast cancer survival improving? Trends in survival for patients with recurrent breast cancer diagnosed from 1974 through 2000. *Cancer*. 2004; 100(1):44–52.
3. Haffty BG, Yang Q, Reiss M, et al. Locoregional relapse and distant metastasis in conservatively managed triple negative early-stage breast cancer. *J Clin Oncol*. 2006; 24(36):5652–5657.
4. Bauer KR, Brown M, Cress RD, Parise CA, Caggiano V. Descriptive analysis of estrogen receptor (ER)-negative, progesterone receptor (PR)-negative, and HER2-negative invasive breast cancer, the so-called triple-negative phenotype: a population-based study from the California Cancer Registry. *Cancer*. 2007; 109(9):1721–1728.
5. Dawood S, Broglio K, Gonzalez-Angulo AM, IV et al. Trends in survival over the past two decades among White and Black patients with newly diagnosed stage breast cancer. *J Clin Oncol*. 2008; 26(30):4891–4898.
6. Hayes DF, Thor AD, Dressler LG, et al. HER2 and response to paclitaxel in node-positive breast cancer. *N Engl J Med*. 2007; 357:1496–1506.
7. Moasser MM. The oncogene HER2: its signaling and transforming functions and its role in human cancer pathogenesis. *Oncogene*. 2007; 26(45):6469–6487.
8. Hurvitz SA, O'Shaughnessy J, Mason G, et al. Central nervous system metastasis in patients with HER2-positive metastatic breast cancer: patient characteristics, treatment, and survival from SystHERs. *Clin Cancer Res*. 2019; 25(8):2433–2441.
9. Leyland-Jones B. Human epidermal growth factor receptor 2–positive breast cancer and central nervous system metastases. *J Clin Oncol*. 2009; 27(31):5278–5286.
10. Niwińska A, Murawska M, Pogoda K. Breast cancer brain metastases: differences in survival depending on biological subtype, RPA RTOG prognostic class and systemic treatment after whole-brain radiotherapy (WBRT). *Ann Oncol*. 2010; 21(5):942–948.
11. Lockman PR, Mittapalli RK, Taskar KS, et al. Heterogeneous blood–tumor barrier permeability determines drug efficacy in experimental brain metastases of breast cancer. *Clin Cancer Res*. 2010; 16(23):5664–5678.
12. DeAngelis LM, Delattre J-YPosner JB. Radiation-induced dementia in patients cured of brain metastases. *Neurology*. 1989; 39(6):789–789.
13. Patchell RA. The management of brain metastases. *Cancer Treat Rev*. 2003; 29(6):533–540.
14. Jakubovic R, Sahgal A, Soliman H, et al. Magnetic resonance imaging-based tumour perfusion parameters are biomarkers predicting response after radiation to brain metastases. *Clin Oncol*. 2014; 26(11):704–712.
15. Teng F, Tsien CI, Lawrence TS, Cao Y. Blood-tumor barrier opening changes in brain metastases from pre to one-month post radiation therapy. *Radiother Oncol*. 2017; 125(1):89–93.
16. Dijkers EC, Oude Munnink TH, Kosterink JG, et al. Biodistribution of 89Zr-trastuzumab and PET imaging of HER2-positive lesions in patients with metastatic breast cancer. *Clin Pharmacol Ther*. 2010; 87(5):586–592.
17. Debie P, Lafont C, Defrise M, et al. Size and affinity kinetics of nanobodies influence targeting and penetration of solid tumours. *J Control Release*. 2020; 317:34–42.
18. Altunay B, Morgenroth A, Beheshti M, et al. HER2-directed antibodies, affibodies and nanobodies as drug-delivery vehicles in breast cancer with a specific focus on radioimmunotherapy and radioimmunoimaging. *Eur J Nucl Med Mol Imaging*. 2021; 48(5):1371–1389.
19. Zhou Z, Vaidyanathan G, McDougald D, et al. Fluorine-18 labeling of the HER2-targeting single-domain antibody 2Rs15d using a residualizing label and preclinical evaluation. *Mol Imaging Biol*. 2017; 19(6):867–877.
20. Keyaerts M, Xavier C, Heemskerk J, et al. Phase I study of 68Ga-HER2-nanobody for PET/CT assessment of HER2 expression in breast carcinoma. *J Nucl Med*. 2016; 57(1):27–33.
21. Pruszynski M, Koumarianou E, Vaidyanathan G, et al. Targeting breast carcinoma with radioiodinated anti-HER2 Nanobody. *Nucl Med Biol*. 2013; 40(1):52–59.
22. Shaw MG, Ball DL. Treatment of brain metastases in lung cancer: strategies to avoid/reduce late complications of whole brain radiation therapy. *Curr Treat Options Oncol*. 2013; 14(4):553–567.
23. Zhang S, Huang W-C, Zhang L, et al. Src family kinases as novel therapeutic targets to treat breast cancer brain metastases. *Cancer Res*. 2013; 73(18):5764–5774.
24. Balyasnikova IV, Prasol MS, Ferguson SD, et al. Intranasal delivery of mesenchymal stem cells significantly extends survival of irradiated mice with experimental brain tumors. *Mol Ther*. 2014; 22:140–148.
25. Dey M, Yu D, Kanojia D, et al. Intranasal oncolytic virotherapy with CXCR4-enhanced stem cells extends survival in mouse model of glioma. *Stem Cell Rep*. 2016; 7(3):471–482.
26. Shi L, Wang D, Liu W, et al. Automatic detection of arterial input function in dynamic contrast enhanced MRI based on affinity propagation clustering. *J Magn Reson Imaging*. 2014; 39(5):1327–1337.
27. Tang L, Zhang H, Zhang B. A note on error bars as a graphical representation of the variability of data in biomedical research: choosing between standard deviation and standard error of the mean. *J Pancreatol*. 2019; 2(3):69–71.
28. Lakens D. Equivalence tests: a practical primer for t tests, correlations, and meta-analyses. *Soc Psychol Personal Sci*. 2017; 8(4):355–362.
29. Choi J, Vaidyanathan G, Koumarianou E, Kang CM, Zalutsky MR. Astatine-211 labeled anti-HER2 5F7 single domain antibody fragment conjugates: radiolabeling and preliminary evaluation. *Nucl Med Biol*. 2018; 56:10–20.
30. D'Huyvetter M, De Vos J, Xavier C, et al. ^{131}I-labeled anti-HER2 Camelid sdAb as a theranostic tool in cancer treatment. *Clin Cancer Res*. 2017; 23(21):6616–6628.
31. D'Huyvetter M, Vos J, Caveliers V, et al. Phase I trial of ^{131}I-GMIB-anti-HER2-VHH1, a new promising candidate for HER2-targeted radionuclide therapy in breast cancer patients. *J Nucl Med*. 2021; 62(8):1097–1105.
32. Puttemans J, Dekempeneer Y, Eersels JL, et al. Preclinical targeted alpha- and beta(-)-radionuclide therapy in HER2-positive brain metastasis using camelid single-domain antibodies. *Cancers (Basel)*. 2020; 12(4):1017.
33. Palmieri D, Bronder JL, Herring JM, et al. Her-2 overexpression increases the metastatic outgrowth of breast cancer cells in the brain. *Cancer Res*. 2007; 67(9):4190–4198.
34. Nanni P, Nicoletti G, Palladini A, et al. Multiorgan metastasis of human HER-2+ breast cancer in Rag2-/-;Il2rg-/- mice and treatment with PI3K inhibitor. *PLoS One*. 2012; 7(6):e39626.
35. Trifiletti DM, Ballman KV, Brown PD, et al. Optimizing whole brain radiation therapy dose and fractionation: results from a prospective phase 3 trial (NCCTG N107C [Alliance]/CEC.3). *Int J Radiat Oncol Biol Phys*. 2020; 106(2):255–260.
36. Brown PD, Jaeckle K, Ballman KV, et al. Effect of radiosurgery alone vs radiosurgery with whole brain radiation therapy on cognitive function in patients with 1 to 3 brain metastases: a randomized clinical trial. *JAMA*. 2016; 316(4):401–409.
37. Chang EL, Wefel JS, Hess KR, et al. Neurocognition in patients with brain metastases treated with radiosurgery or radiosurgery plus

whole-brain irradiation: a randomised controlled trial. *Lancet Oncol.* 2009; 10(11):1037–1044.

38. Schulz M, Michels B, Niesel K, et al. Cellular and molecular changes of brain metastases-associated myeloid cells during disease progression and therapeutic response. *iScience.* 2020; 23(6):101178.
39. Svensson JP, Stalpers LJ, Esveldt-van Lange RE, et al. Analysis of gene expression using gene sets discriminates cancer patients with and without late radiation toxicity. *PLoS Med.* 2006; 3(10):e422.
40. Dilworth JT, Krueger SA, Dabjan M, et al. Pulsed low-dose irradiation of orthotopic glioblastoma multiforme (GBM) in a pre-clinical model: effects on vascularization and tumor control. *Radiother Oncol.* 2013; 108(1):149–154.
41. Yuan H, Gaber MW, Boyd K, et al. Effects of fractionated radiation on the brain vasculature in a murine model: blood-brain barrier permeability, astrocyte proliferation, and ultrastructural changes. *Int J Radiat Oncol Biol Phys.* 2006; 66(3):860–866.
42. Warrington JP, Ashpole N, Csiszar A, et al. Whole brain radiation-induced vascular cognitive impairment: mechanisms and implications. *J Vasc Res.* 2013; 50(6):445–457.
43. Zeng YD, Liao H, Qin T, et al. Blood-brain barrier permeability of gefitinib in patients with brain metastases from non-small-cell lung cancer before and during whole brain radiation therapy. *Oncotarget.* 2015; 6(10):8366–8376.
44. Murrell DH, Hamilton AM, Mallett CL, et al. Understanding heterogeneity and permeability of brain metastases in murine models of HER2-positive breast cancer through magnetic resonance imaging: implications for detection and therapy. *Transl Oncol.* 2015; 8(3):176–184.
45. Adkins CE, Mohammad AS, Terrell-Hall TB, et al. Characterization of passive permeability at the blood-tumor barrier in five preclinical models of brain metastases of breast cancer. *Clin Exp Metastasis.* 2016; 33(4):373–383.
46. Leone JP, Leone BA. Breast cancer brain metastases: the last frontier. *Exp Hematol Oncol.* 2015; 4:33.
47. Mittapalli RK, Adkins CE, Bohn KA, et al. Quantitative fluorescence microscopy measures vascular pore size in primary and metastatic brain tumors. *Cancer Res.* 2017; 77(2):238–246.
48. Feng Y, Meshaw R, McDougald D, et al. Evaluation of an ^{131}I-labeled HER2-specific single domain antibody fragment for the radiopharmaceutical therapy of HER2-expressing cancers. *Sci Rep.* 2022; 12(1):3020.